

# Global Biogeochemical Cycles®






## RESEARCH ARTICLE

10.1029/2023GB008018

### Special Collection:

The U.S. GEOTRACES Pacific Meridional Transect (GP15)

## Biogeochemical Fluxes of Nickel in the Global Oceans Inferred From a Diagnostic Model

Seth G. John<sup>1</sup> , Hengdi Liang<sup>1</sup> , Benoît Pasquier<sup>1,2</sup> , Mark Holzer<sup>2</sup> , and Sam Silva<sup>1</sup> 

<sup>1</sup>Department of Earth Sciences, University of Southern California, Los Angeles, CA, USA, <sup>2</sup>School of Mathematics and Statistics, University of New South Wales, Sydney, NSW, Australia

### Key Points:

- A diagnostic model shows that surface ocean Ni uptake is coupled to P uptake, and does not slow when Ni concentrations approach 2 nM
- Ni regeneration is deeper in the ocean than P remineralization, suggesting slower remineralization or reversible scavenging
- The approach described here for diagnostic modeling complements approaches based on prognostic biogeochemical models

### Correspondence to:

S. G. John,  
[sethjohn@usc.edu](mailto:sethjohn@usc.edu)

### Citation:

John, S. G., Liang, H., Pasquier, B., Holzer, M., & Silva, S. (2024). Biogeochemical fluxes of nickel in the global oceans inferred from a diagnostic model. *Global Biogeochemical Cycles*, 38, e2023GB008018. <https://doi.org/10.1029/2023GB008018>

Received 16 NOV 2023

Accepted 13 APR 2024

### Author Contributions:

**Conceptualization:** Seth G. John, Benoît Pasquier

**Formal analysis:** Hengdi Liang

**Funding acquisition:** Seth G. John

**Investigation:** Seth G. John

**Methodology:** Seth G. John,

Benoît Pasquier, Mark Holzer, Sam Silva

**Project administration:** Seth G. John

**Software:** Seth G. John, Hengdi Liang,

Benoît Pasquier, Mark Holzer

**Supervision:** Seth G. John

**Validation:** Seth G. John, Hengdi Liang, Sam Silva

**Visualization:** Seth G. John, Hengdi Liang

**Writing – original draft:** Seth G. John,

Benoît Pasquier, Mark Holzer, Sam Silva

**Writing – review & editing:** Seth G. John,

Hengdi Liang, Benoît Pasquier,

Mark Holzer, Sam Silva

**Abstract** Nickel (Ni) is a micronutrient that plays a role in nitrogen uptake and fixation in the modern ocean and may have affected rates of methanogenesis on geological timescales. Here, we present the results of a diagnostic model of global ocean Ni fluxes which addresses key questions about marine Ni cycling. Sparsely available observations of Ni concentration are first extrapolated into a global gridded climatology using tracers with better observational coverage such as macronutrients, and testing three different machine learning techniques. The physical transport of Ni is then estimated using the ocean circulation inverse model (OCIM2), revealing regions of net convergence or divergence. These diagnostics are not based on any assumption about Ni biogeochemical cycling, but their spatial patterns can be used to infer where biogeochemical processes such as biological Ni uptake and regeneration take place. Although Ni and silicate (Si) have similar concentration patterns in the ocean, we find that the spatial pattern of Ni uptake in the surface ocean is similar to phosphate (P) uptake but not to silicate (Si) uptake. This suggests that their similar distributions arise from different biogeochemical mechanisms, consistent with other evidence showing that Ni is not incorporated into diatom frustules. We find that Ni:P ratios at uptake do not decrease as Ni concentrations approach 2 nM, which challenges the hypothesis of a ~2 nM pool of non-bioavailable Ni in the surface ocean. Finally, we find that the net regeneration of Ni occurs deeper in the ocean than for P, though not as deeply as for Si.

**Plain Language Summary** Nickel is an important micronutrient for algae that live in the oceans. Here, we have built a computer model that predicts where phytoplankton (microscopic algae living in the surface ocean) take nickel out of seawater in the surface ocean, and where they release nickel back into the dissolved phase after they die and sink into the ocean abyss. To build this model, we first needed to predict the nickel concentration in global oceans based on a few simple parameters such as temperature, salinity, and the concentration of other nutrients. We then used our model output to answer the following open questions about nickel cycling: Which species of phytoplankton take nickel out of seawater? Do hard-shelled diatoms (an important type of phytoplankton) incorporate nickel into their shells? Is nickel removed from the dissolved phase by chemically sticking onto sinking particles in the ocean?

## 1. Introduction

### 1.1. The Cycling of Ni in the Global Oceans

Nickel (Ni) is a nutrient for phytoplankton in the oceans. It is a cofactor for important enzymes including Ni superoxide dismutase (NiSOD), which detoxifies superoxide radicals (Alfano & Cavazza, 2020; Dupont et al., 2008; Qiu & Price, 2009), urease, which facilitates uptake of the nitrogen from the N-containing molecule urea (Alfano & Cavazza, 2020; Biscéré et al., 2018; Dupont et al., 2008), and NiFe hydrogenase, which catalyzes the reaction of hydrogen gas to protons and electrons and is involved in nitrogen fixation (Tuo et al., 2020). Nickel is also crucial for methanogenesis as a cofactor for the enzyme methyl-coenzyme M reductase (MCR), leading to the speculation that Ni availability in the past oceans played a key role in controlling methanogenesis, and therefore oxygenation of the atmosphere (Konhauser et al., 2009; Wang et al., 2019; Zhao et al., 2021).

Nickel has a nutrient-like distribution in the oceans. It is depleted in the surface ocean compared to the deep ocean, and it exhibits increasing concentrations from the deep Atlantic to the deep Pacific Ocean (Figure 1), which is characteristic of elements that are incorporated into biological tissue in the surface ocean and regenerated at depth where they accumulate along the deep ocean “conveyor belt” (GEOTRACES Intermediate Data Product Group, 2021; John & Sunda, 2018; Schlitzer et al., 2018). While these broad patterns in the global distribution of

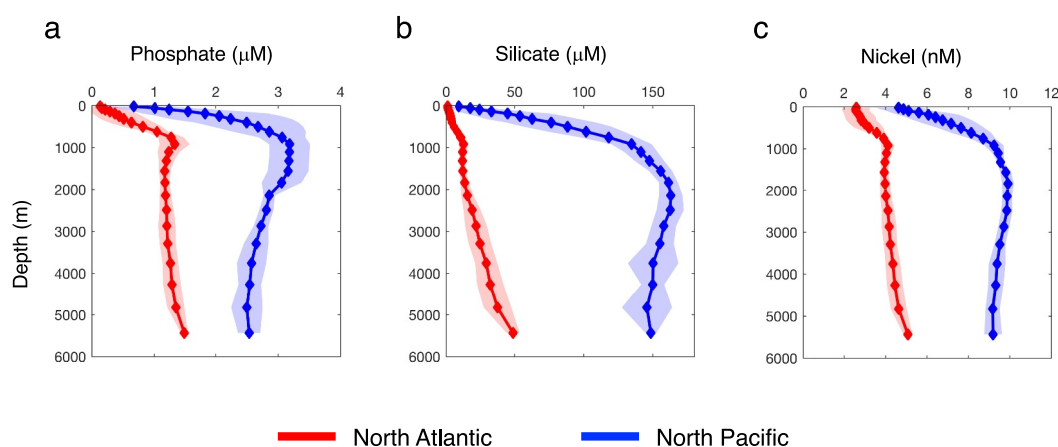


**Figure 1.** Phosphate (a), silicate (b), and nickel (c) concentrations in the North Atlantic and North Pacific oceans between 35° N and 65.6°N, taken from the GEOTRACES 2017 Intermediate Data Product. Shaded regions represent the 1 $\sigma$  standard deviation of all data within the region.

Ni are easily explained, key details of Ni biogeochemical cycling are still debated, including whether Ni is incorporated into diatom frustules and whether all Ni in the surface oceans is bioavailable.

## 1.2. Two Key Hypotheses for the Marine Biogeochemical Cycle of Ni

The first hypothesis is that Ni is incorporated into diatom frustules. This hypothesis was first suggested based on the deeper regeneration maximum of Ni compared to soft-tissue elements N and P (Bruland, 1980). This hypothesis received further support based on spatial analysis of the distribution of elements within individual diatom cells using synchrotron X-ray fluorescence (SXRF) mapping, that shows large amounts of Ni are present on the outside of diatoms in the same location where Si from diatom frustules is observed (Twining et al., 2012). Also, the addition of silicate (Si) to equatorial waters promoted a large drawdown in Ni, further suggesting that Ni could be incorporated into diatom frustules (Twining et al., 2012). Incorporation of Ni into the opal silicate matrix of diatom frustules, and slow release of Ni as sinking frustules dissolve could explain all these observations.

However, recent work suggests that Ni is not present in diatom frustules. John et al. (2022) found that nearly all of the Ni in both laboratory-cultured and natural diatoms is present in the nitric acid (HNO<sub>3</sub>) soluble soft-tissue, rather than in the hydrofluoric acid (HF) soluble silicate frustules. Using a recent biogeochemical model, they were able to reproduce the Si-like deep regeneration of Ni either through reversible scavenging of Ni onto sinking particulate matter or through slower regeneration of Ni compared to P.

The second key hypothesis is the existence of a refractory (i.e., non-bioavailable) Ni pool. Nickel is never depleted below ~1.7 nM, compared to maximum deep concentrations around 10 nM, while macronutrients N, P, and Si and many other trace-metals such as Fe, Zn, and Cd are depleted by orders of magnitude compared to their deep ocean maxima (John & Sunda, 2018). However, the uptake of Ni in the high-latitudes only depletes Ni down to concentrations around ~1.7 nM in the oligotrophic gyres, leading to the suggestion that Ni is comprised of biologically available pool that dominates in the deep ocean, and a separate ~2 nM non-bioavailable pool of Ni that is never depleted in the surface ocean (Mackey et al., 2002; Price & Morel, 1991; Wen et al., 2006). A ~2 nM non-bioavailable pool of Ni has also been invoked to explain patterns of Ni isotopes in the surface oceans that are anomalously high at lower Ni concentrations compared to what would be expected based on simple Rayleigh fractionation, but could be explained by mixing of bioavailable and non-bioavailable pools of Ni with different  $\delta^{60}\text{Ni}$  signatures (Archer et al., 2020; Lemaitre et al., 2022).

Recent experimental and modeling work calls into question the existence of a non-bioavailable Ni pool. Specifically, it has been shown that Ni in natural seawater is chemically labile to EDTri-A functional groups on Nobias resin, and is biologically available to several species of cyanobacteria and diatoms in culture when the seawater culture media is amended with extra macronutrients, with both experiments showing that Ni can be drawn down well below the ~2 nM threshold (John et al., 2022). These observations can be reconciled with the lack of Ni depletion in oligotrophic gyres by a biogeochemical model in which Ni is depleted slightly more slowly

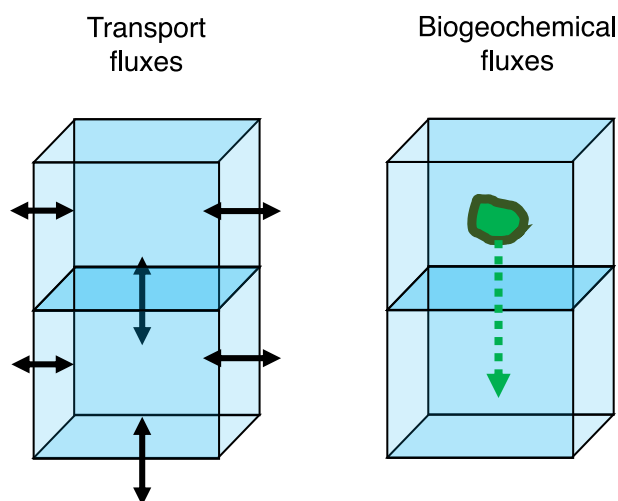


**Figure 2.** The diagnostic modeling approach first calculates the steady-state transport fluxes of the dissolved element into and out of every model grid cell with water mixing and advection. Any net gain or loss of the element from physical transport can subsequently be attributed to a biogeochemical process, such as loss of a nutrient element from surface boxes by incorporation into phytoplankton biomass and sinking of those particles, or a source of the element in the deeper ocean due to particle remineralization.

than macronutrients from upwelling waters, such that the  $\sim 2$  nM Ni observed in oligotrophic gyres is simply the amount of Ni that is “left over” after macronutrient depletion.

### 1.3. Prognostic and Diagnostic Models

The only previous effort to model Ni in the global oceans, of which we are aware, is a mechanistic biogeochemical model or a “prognostic” model built using the AWESOME OCIM framework (S. G. John et al., 2020). This model included the processes of biological uptake and remineralization of soft-tissue Ni, and in some cases reversible scavenging of Ni onto sinking particles, all occurring within the realistic global ocean circulation prescribed by OCIM 1.0 (the Ocean Circulation Inverse Model; DeVries, 2014). This prognostic model was able to skillfully reproduce the global distribution of Ni in the global oceans ( $R^2 = 0.95$ ) and was useful in evaluating the hypotheses described above within a numerical modeling framework.

A different approach for exploring the biogeochemical processes that cycle elements in the ocean is to use what we here call a “diagnostic” model. Instead of explicitly parameterizing every biogeochemical process, a diagnostic model infers them by other means. Specifically, it is possible to determine if biogeochemical processes add or remove a metal from the dissolved phase from the spatial patterns of other tracers and/or using a model of the ocean circulation. With the advent of global-scale trace-metal sampling programs

such as GEOTRACES, it has become possible to build such diagnostic models for metals, as has been successfully done for Zn (Roshan et al., 2018), Cu (Roshan et al., 2020), and Cd (Roshan & DeVries, 2021).

The diagnostic modeling approach used here is to calculate the transport of Ni by physical circulation, and to infer biogeochemical fluxes of nutrients from any imbalance between transport sources and sinks (Figure 2). The ocean circulation model completely determines the movement of water between neighboring grid cells. Thus, if the Ni concentration in every model grid cell is known, it becomes possible to calculate the rate at which Ni is being transported into and out of every grid cell.

When performing such calculations for ocean nutrients, it is typical to find a net supply of nutrients into surface ocean grid cells by water transport (Weber & Deutsch, 2010; Weber et al., 2016). This occurs because surface ocean nutrient concentrations are low, while concentrations in nearby subsurface grid cells are higher, so that exchange of water between the surface and subsurface ocean grid cells results in a net upward flux of dissolved nutrients. Conversely, grid cells deeper in the ocean typically experience a net loss of nutrients by physical transport. As described below, the maintenance of steady-state nutrient distributions in the ocean thus requires invoking additional processes such as the removal of nutrients from surface waters by phytoplankton uptake, and the addition of nutrients into the deep ocean by remineralization.

Sources and sinks of tracers due to physical water transport can be described using various terminologies. For example, one might describe a net supply of dissolved nutrients into the surface ocean by water transport as a “transport flux convergence.” Alternatively, it is common in modeling and engineering to describe flux in terms of their divergences, in which case it would be most accurately described as a “negative net transport flux divergence.” Colloquially, this could be described as a net supply of nutrients to the surface ocean by transport. In the deep ocean, nutrient elements typically have a positive net transport flux divergence, corresponding to a net loss of nutrients by water transport. A similar approach is widely used in oceanography to determine heat fluxes into and out of the surface ocean, which are calculated in terms of the deviations from the heat transport convergence (Grist et al., 2010; Sutton & Mathieu, 2002; Zanna et al., 2019).

Because of mass conservation, in steady state the external sources (e.g., remineralization) and sinks (e.g., biological uptake) of a dissolved tracer must balance its flux divergence due to physical circulation. We emphasize that the key feature of this diagnostic modeling approach is that it does not involve any explicit biogeochemistry calculation. That is, the flux divergence is calculated at every grid cell and highlights the spatial regions over which a tracer must be added or removed to be in balance, without any assumptions about what sorts of

biogeochemical processes would account for this addition or removal. Nonetheless, such calculations of transport divergences often have obvious biogeochemical interpretations. For example, the negative net transport divergence in the surface ocean reflects the uptake of an element by phytoplankton, while the positive net transport divergence in the deep ocean reflects remineralization.

Building a diagnostic model such as described above requires knowledge of the concentration of dissolved Ni in every model grid cell. This is typically straightforward for macronutrients and other fields for which global climatologies are available (e.g., the World Ocean Atlas). However, even with the dramatic increase in the availability of trace-metal concentration data from the GEOTRACES program (GEOTRACES Intermediate Data Product Group, 2021; Schlitzer et al., 2018), global climatologies for most trace metals are not yet available. Thus, diagnostic models of trace-metal cycling first require an extrapolation for determining the global distribution of the element, which can be accomplished by machine-learning, for example, using Artificial Neural Networks (ANNs) (Roshan & DeVries, 2021; Roshan et al., 2018, 2020).

Here, we present a new diagnostic model of Ni fluxes in the global ocean. This model is used to further explore key questions regarding the global Ni cycle, such as whether Ni is significantly incorporated into diatom frustules, causes of the relatively deep concentration maximum observed for Ni, and whether Ni in surface ocean oligotrophic gyres is bioavailable. This work thus complements an earlier prognostic model of Ni biogeochemical cycling (John et al., 2022) by using a very different modeling approach.

## 2. Methods

### 2.1. General Approach

This project was carried out in a combination of modeling environments and languages. Machine learning predictions of Ni concentrations in the global ocean were performed in MATLAB using tools available as part of the AWESOME OCIM modeling environment (S. G. John et al., 2020). OCIM circulations are produced starting with global geostrophic flow calculations, and then further tuned to match the distribution of CFCs, radiocarbons, temperature, salinity, and other tracers to yield a realistic representation of how circulation affects the distribution of tracers in the ocean interior (DeVries & Primeau, 2011; DeVries & Holzer, 2019a; S. G. John et al., 2020). Nutrient-restoring and boundary-condition modeling was performed using the Algebraic Implicit Biogeochemical Elemental Cycling System (AIBECS) modeling framework (Pasquier, 2019). Like the AWESOME OCIM, AIBECS is designed for users to write and run their own biogeochemical models using transport-matrix techniques. Specific advantages of AIBECS are that it is written in the open-source Julia programming language, that it is designed to easily run the same biogeochemical model with multiple different circulation transport matrices, that it can run models with non-linear biogeochemical equations, and that biogeochemical equations can be input from a single interface using traditional mathematical symbology. After running our model in AIBECS, the output was then imported back into MATLAB/AWESOME OCIM for additional data processing and plotting.

### 2.2. Producing a Global Climatology of Dissolved Ni

Machine learning techniques provide a way to extrapolate sparse Ni observations to predict the Ni concentration at every point of a global ocean model grid. In the past, such techniques have been used to predict global climatologies of other trace-elements including Zn (Roshan et al., 2018), Cu (Roshan et al., 2020), Cd (Roshan & DeVries, 2021), Fe (Huang et al., 2022), and Ba (Metz et al., 2023).

Here we started with Ni concentration data as reported in the GEOTRACES Intermediate Data Product 2021 (Boiteau et al., 2016; GEOTRACES Intermediate Data Product Group, 2021; Middag et al., 2020; Minami et al., 2015; Zheng et al., 2021). Placing these data onto the model grid, and averaging all points within each model grid cell yields 4,756 grid cells with Ni concentration out of the total 200,160 “wet” model grid cells, or a little more than 2%. Predictors used in the machine learning algorithms included World Ocean Atlas 2009 climatologies of nitrate, phosphate, silicate, oxygen, salinity, and temperature, as well as depth, and the sine and cosine of latitude. Normalization was performed on the predictors before fitting the regression models. Standardization was done by subtracting the mean and dividing by the standard deviation of each predictor variable, allowing for a fair comparison of the coefficients, and facilitating the interpretation of their magnitudes. Normalization scaled the predictors to a range between 0 and 1, preventing the dominance of any single predictor.

Three different methods were explored for their ability to reproduce observed Ni, and extrapolate to create global Ni climatologies, including multiple linear regression (MLR), artificial neural networks (ANNs), and decision trees. Each of these three methods was tested by creating three sets of experiments using the Matlab fitlm, fitrnet, and fitrtree functions. The models were first trained on Ni concentration observations from one ocean basin (Atlantic or Pacific) and then validated with Ni concentration observations from another ocean basin (Pacific or Atlantic) to assess how well the model performs with new, unseen data. Finally, the full data set of GEOTRACES Ni observations was utilized to generate a global climatology of dissolved Ni.

All three models performed with a similar level of skill with the training data set of all global data, with slopes for a comparison of predicted and observed Ni between 0.94 and 0.99 and  $R^2$  values between 0.94 and 0.99. Similarly, all three models produced a good fit with  $R^2 > 0.9$  when using the entire global data set as both the training set and validation set. However, when predicting a validation Ni data set in one ocean basin using a training data set from a different ocean basin (e.g., using Atlantic data to predict Ni in the Pacific, or vice versa), both the ANN and decision tree methods sometimes produce very poor results (Figure 3). For example, the ANN model approach was used six times because randomization produces different results each time, with highly variable skill in predicting the validation data set ( $R^2$  0.26, -0.28, 0.94, 0.59, 0.78, and 0.55). The decision-tree model also produced poor results for the validation sets ( $R^2$  0.81 and 0.53). Both techniques were particularly prone to errors when predicting high Ni concentrations in the deep Pacific when trained on Ni data from the Atlantic, which did not contain any such high values. The MLR model appeared least prone to producing spurious data for the validation data set, with  $R^2 > 0.90$  for the validation data sets when predicting the Pacific Ni concentrations from Atlantic data, and vice versa. The linear model has a good fit to Ni observations over a wide spatial range ( $R^2 = 0.94$ , Figures 3 and 4), and is also the simplest model. Thus, we chose the MLR model to produce the global Ni climatology upon which the restoring model was built.

### 2.3. Smoothing Nutrient Distributions With a Restoring Model

Given a global climatology of nutrient distribution and a circulation transport matrix, it should be possible, in theory, to directly calculate flux convergences for every model grid cell. In practice, however, combining raw “observational” climatologies such as those from the World Ocean Atlas or our extrapolated Ni coverage, and OCIM circulations produces results with significant numerical noise, and does not provide useful information even after averaging over large spatial regions. Thus, it is necessary to practice to first generate OCIM-compatible climatologies. These climatologies are smoother than the original climatologies from the World Ocean Atlas (for phosphate and silicate) or from the machine learning prediction (for Ni), but more importantly, these climatologies are consistent with grid-scale variability in water mixing and transport present with OCIM circulation matrices.

These climatologies are produced using a restoring model with a set timescale. As the name implies, a restoring model works to restore values toward some baseline, which in this case is the observed climatology or machine learning predicted climatology. At the same time, the restoring model allows circulation to mix the tracer throughout the ocean. The degree of restoration which occurs thus depends on the timescale ( $\tau$ ) over which values are restored to the climatology; a restoring timescale of zero would yield a tracer field exactly the same as the original observations or climatology, while a very large timescale (much greater than the millennial mixing timescale of the oceans) would homogenize tracer concentrations throughout the global ocean. An intermediate timescale produces a new tracer distribution which is smoother than the original but retains its key biogeochemical characteristics. Mathematically focused descriptions of nutrient restoring models are presented in the work of Roshan, DeVries and coauthors (2015; 2017; 2018; 2021).

From a more practical perspective, OCIM-compatible climatologies of Ni, phosphate, and silicate were created with nutrient restoring models built within AIBECS (Figure 5). Using AIBECS, the concentration of tracer  $x$  is computed by restoring it toward the observed value in each grid cell ( $x_{\text{obs}}$ ) via the tracer equation:

$$dx/dt = 0 = -\mathbf{T}x + \frac{x - x_{\text{obs}}}{\tau_{\text{surf}}}(x \geq x_{\text{obs}})(z \leq z_{\text{surf}}) + \frac{x - x_{\text{obs}}}{\tau_{\text{deep}}}(z \leq z_{\text{surf}}) \quad (1)$$

where  $-\mathbf{T}x$  is the transport flux divergence by physical circulation,  $z_{\text{surf}}$  is the depth separating the surface and deep oceans, and  $\tau_{\text{surf}}$  and  $\tau_{\text{deep}}$  are the restoring timescales in the surface and deep oceans, respectively. The flux-

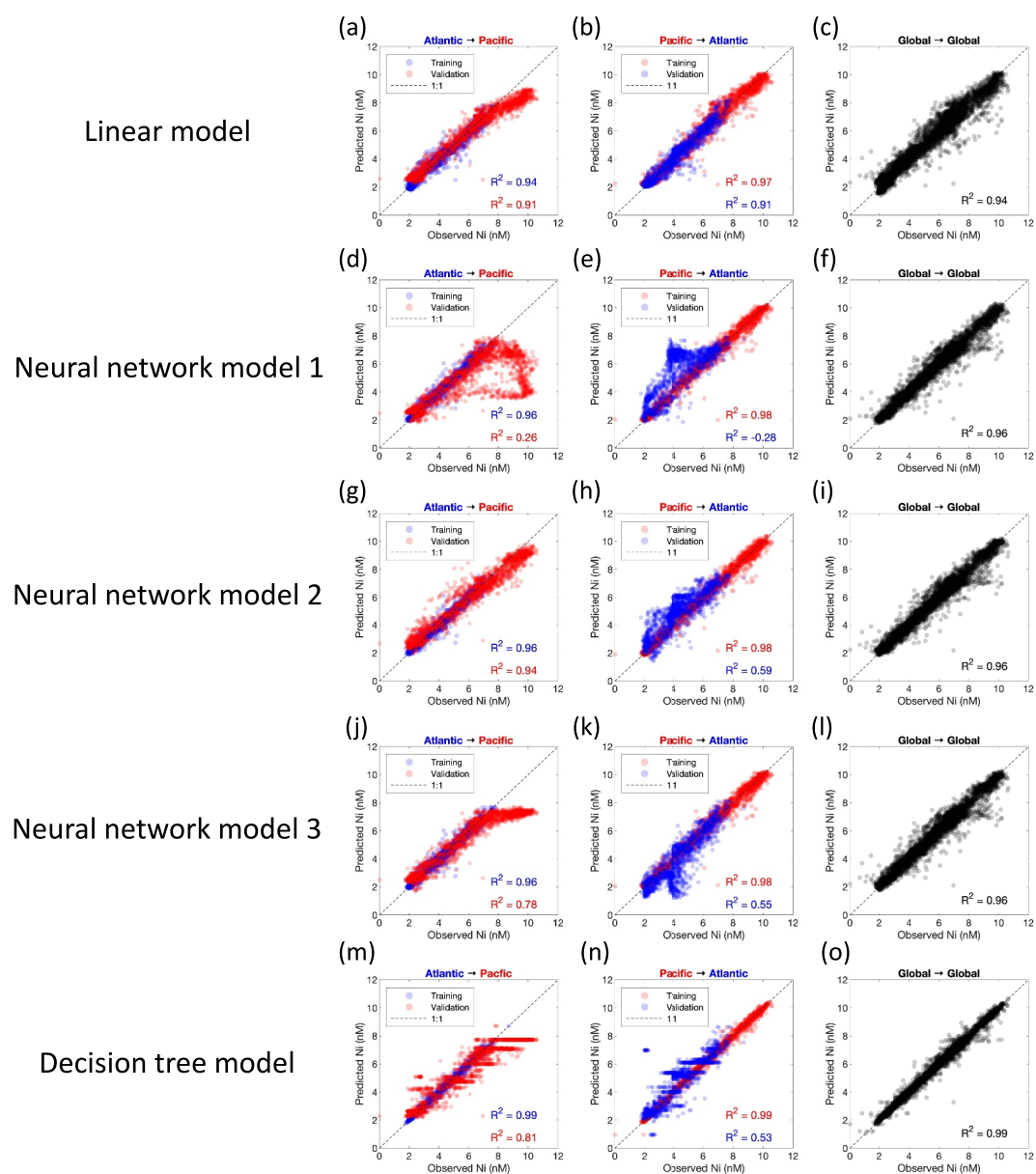


**Figure 3.** Three different types of models (multiple linear regression (MLR), artificial neural network (ANN), and decision tree) were used to predict the concentrations of Ni in the oceans. For each model, we tested predictions of Pacific Ocean validation data using Atlantic Ocean data to train the model, predictions of Atlantic Ocean validation data using Pacific Ocean data to train the model, and predictions of global ocean Ni when the entire global data set was used for both training and validation. Results from multiple ANN models are shown because randomization in the ANN routine leads to slightly different results each time.

divergence term  $-T_x$  allows concentrations to mix and homogenize between nearby model grid cells, while the restoring timescales  $\tau_{\text{surf}}$  and  $\tau_{\text{deep}}$  restore model concentrations back to observations by pushing  $x$  toward  $x_{\text{obs}}$ . The constraint ( $x \geq x_{\text{obs}}$ ) assures that there is no biological uptake taking place in the surface ocean when the simulated tracer concentration is already lower than observations, and thus negative concentrations are not created.

#### 2.4. Calculating the Global Transport Divergences

Transport flux divergences for Ni, phosphate, and silicate were calculated 200 times using a random assortment of parameters in order to create the OCIM-compatible climatologies. For each run of the nutrient restoring model, 1

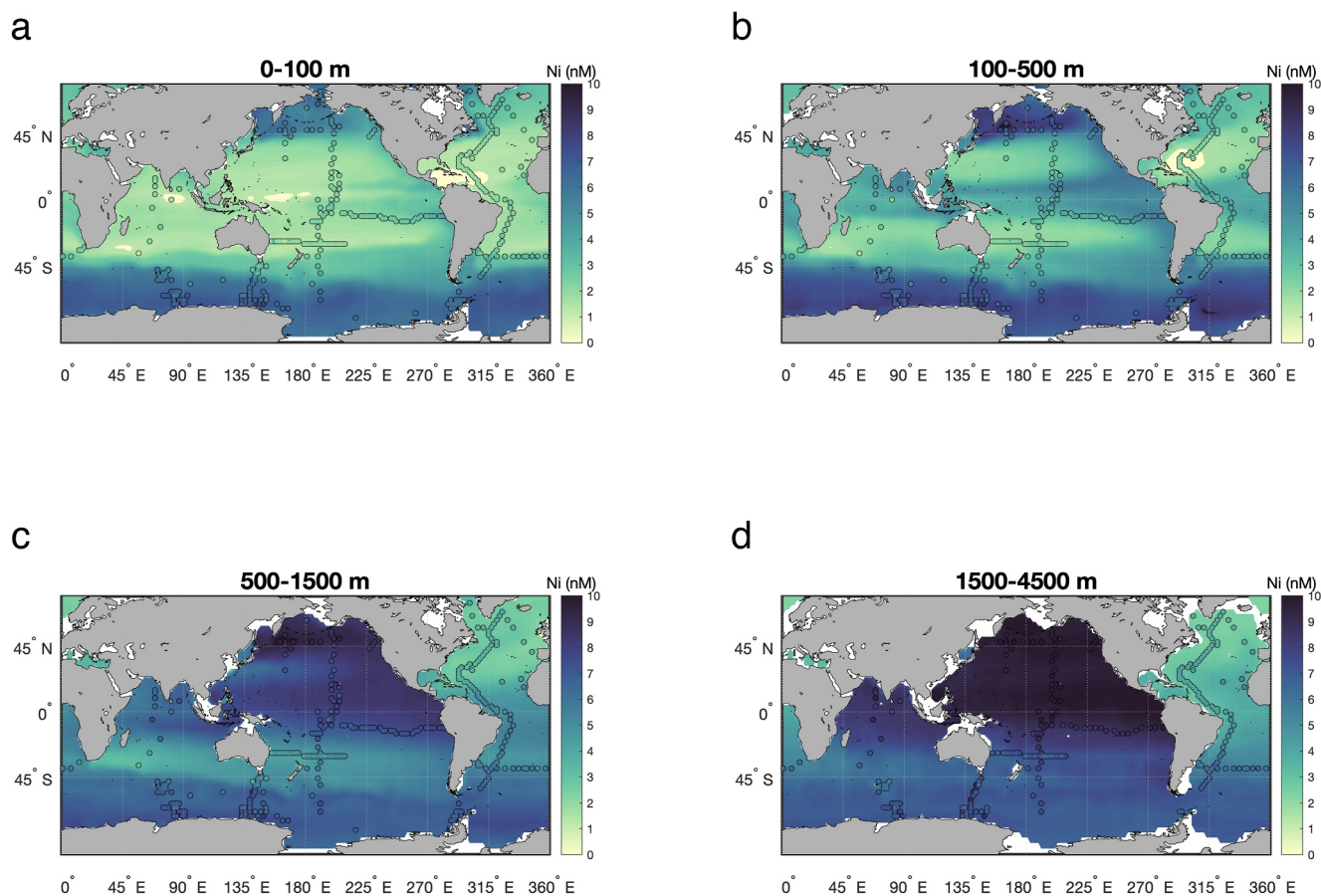


**Figure 4.** Nickel observations from the 2021 GEOTRACES Intermediate Data Product (circles) are compared with Ni concentrations predicted from the multiple linear regression (MLR) model, shown here averaged over different depth ranges.

of 10 OCIM 2 climatologies was chosen (DeVries & Holzer, 2019b): a value between 1 and 9 months for  $\tau_{\text{surf}}$ , a value between 5 and 20 years for  $\tau_{\text{deep}}$ , and a value of  $z_{\text{surf}}$  of either 74 or 114 m, corresponding to either the upper 2 or 3 model layers. These values roughly span the ranges in temporal and spatial scales over which biogeochemical patterns emerge in the surface and deep oceans (Roshan and DeVries, 2017, 2021; Roshan et al., 2018; Roshan & Wu, 2015). Comparing the full range of these parameters shows that similar results are obtained for any values within the range. Because the residence time of Ni in the oceans ( $\sim 20,000$  years) is much longer than the circulation mixing time of the ocean, external sources and sinks will have a minimal impact on Ni distributions and can be neglected here (Little et al., 2020).

For each of these sets of parameters, the climatology was created for Ni, phosphate and silicate using the nutrient-restoring model described above. This climatology ( $\mathbf{x}$ ) was then multiplied by the transport matrix ( $-\mathbf{T}$ ) in order to estimate the transport flux divergence. The 200 transport flux divergence estimates were averaged together to provide an average global distribution of transport flux divergences, which are used as the basis for further interpretation (Figure 6).

### 3. Results and Discussion

#### 3.1. The Factors Predicting Ni Concentrations in the Oceans

Both MLR and decision-tree models provide a framework for evaluating which factors are most important for predicting Ni concentrations. It is important to note that this only reflects the importance of that factor in predicting Ni concentrations, and does not necessarily imply that the factor has a causal impact on Ni concentrations. Indeed, factors of high predictive importance may simply be impacted by another important process (such as biological uptake) in similar ways, or could even have a purely co-incidental relationship.

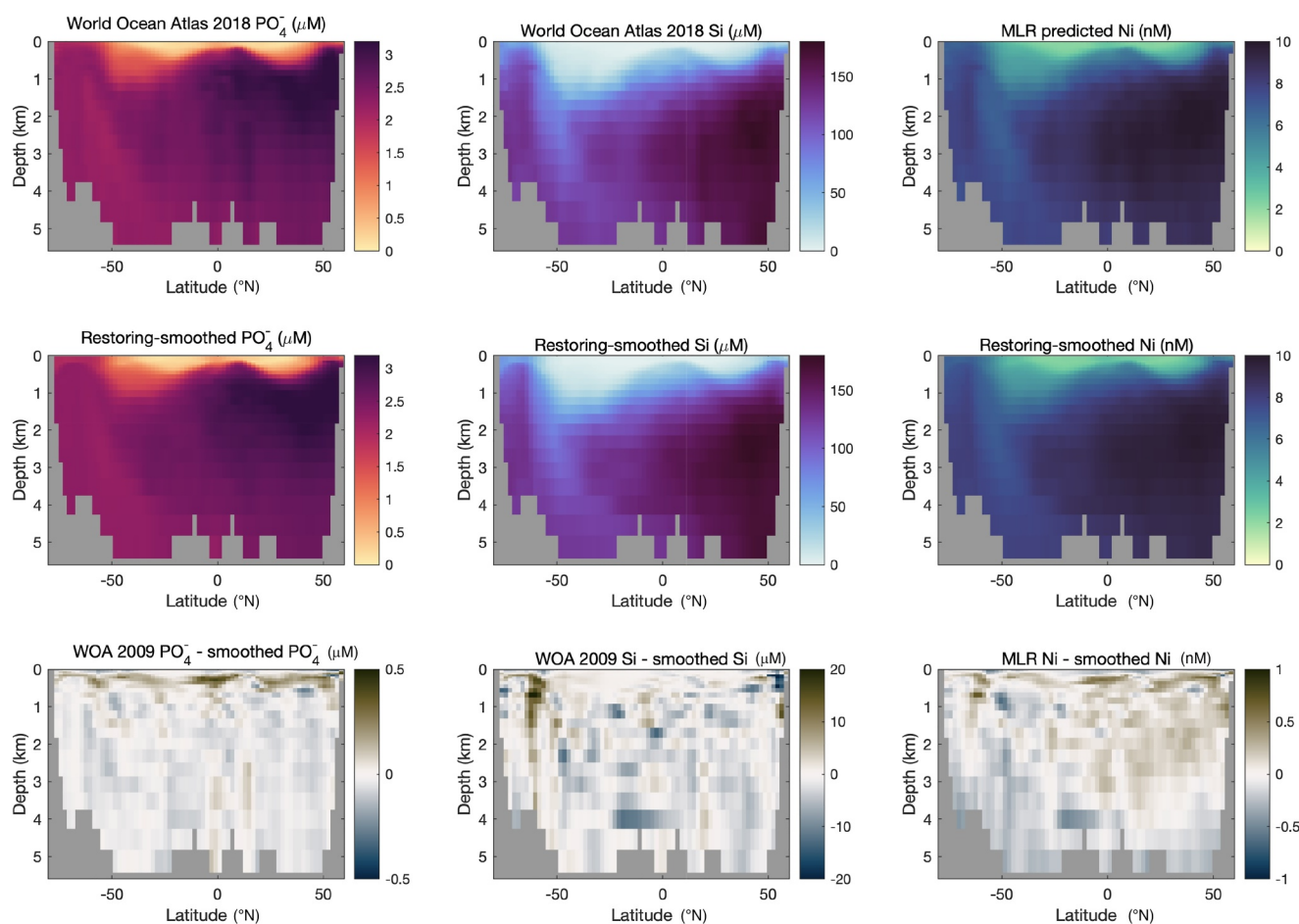


**Figure 5.** A comparison of the observational data before and after processing through a nutrient-restoring model. Phosphate and silicate data from the 2009 World Ocean Atlas are gridded onto the OCIM model grid, while nickel is predicted using a multiple linear regression. All data are shown along a single representative transect through the Pacific Ocean at 161°W, and smoothing-restored distributions reflect the model output from a single run of the nutrient-restoring model.

For the multiple linear regression model, we assess the most important predictors based on the coefficients of each standardized and normalized variable in the linear regression equation (Table 1). We find that silicate is the most important predictor for Ni concentration with a positive coefficient of 1.4 while the second most important predictor is phosphate with a similar coefficient of 1.3. The relative importance of different factors in the decision tree algorithm is calculated based on the summed mean-square error due to splits on every predictor, divided by the total number of branch nodes. The three most important predictors were the macronutrients nitrate, silicate, and phosphate (0.003, 0.0006, 0.0004, respectively). This result, when combined with the MLR outcome, is consistent with the observation that the distribution of oceanic Ni is intermediate between the distributions of nitrate and silicate.

### 3.2. Surface Ocean Uptake Patterns

The net transport flux divergence of Si is negative in the surface oceans, reflecting the supply of Si to the surface ocean by water transport, and being interpreted here as biological Si uptake. This transport flux is, as expected, most intense in the surface ocean at high latitudes (Figures 6 and 7). Si uptake is highest between roughly 80°S and 60°S and decreases northward between 60°S and 40°S, with near-zero uptake across the oligotrophic gyres and equator. This reflects the rapid biological uptake of Si by diatoms in cold, upwelling high-latitude waters.

Similarly, the transport flux divergence of phosphate and Ni in the surface ocean is highest at high latitudes but is more evenly distributed across latitudes (Figures 6 and 7). The zonally averaged biological uptake of Ni and phosphate do not approach zero as closely as Si in subtropical latitudes, and have a noticeable increase at the



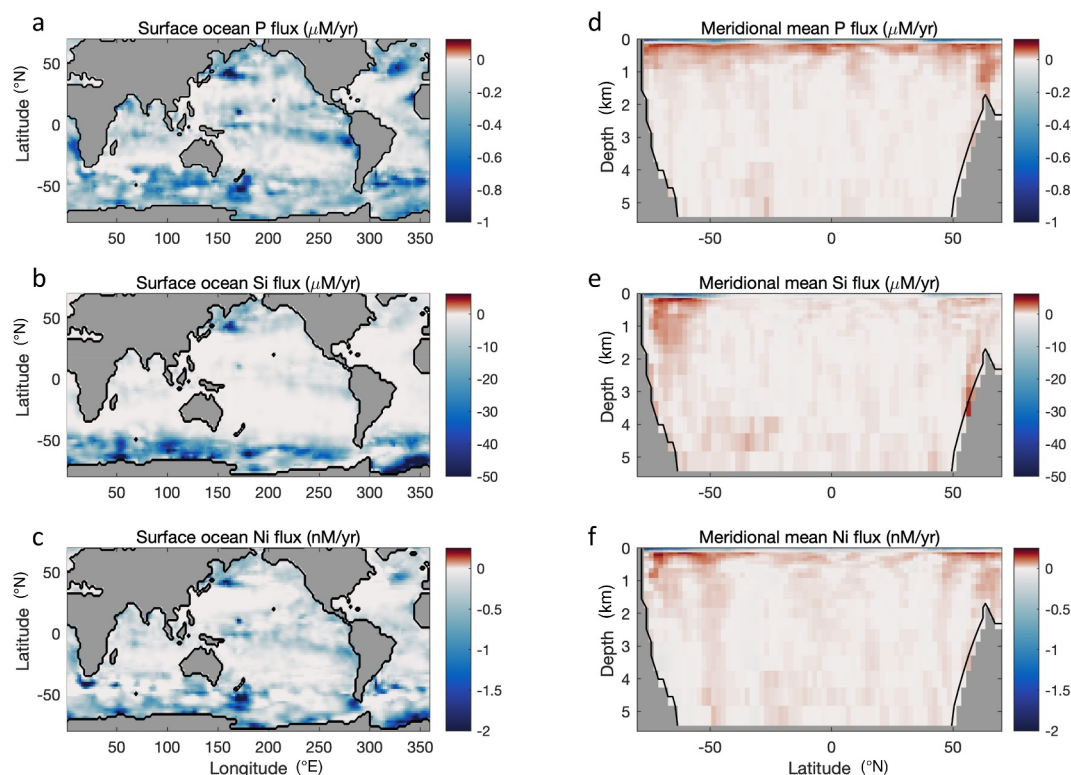


**Figure 6.** Global ocean fluxes of phosphate, silicate and nickel are calculated as the transport divergence, such that a negative transport divergence in the surface ocean reflects net supply by transport and can be interpreted as being balanced by biological uptake, and the positive transport divergences in the deeper ocean reflect net removal by transport and are interpreted as reflecting input from regeneration. All color scales are linear. Note that negative (blue) fluxes appear at the shallowest depths on the meridional transects.

equator, presumably reflecting enhanced productivity driven by equatorial upwelling. An overall similarity in the patterns of Ni and P uptake is seen when directly comparing their uptake rates as a ratio (Figure 7d), with the relative uptake rates varying between 1 and 3 (nM/μM), but there is no clear pattern in the latitudinal distribution of this ratio. In contrast, the ratio of Ni uptake compared to Si uptake has a clear latitudinal pattern, being greatly depressed at high latitudes and greatly enhanced at tropical and subtropical latitudes. These features support the

**Table 1**  
*The Importance of Various Predictors Used in the Multiple Linear Regression and Decision Tree Models, Reported as the Value of the Coefficients of the Standardized and Normalized Predictors for Linear Model and the Predictor Importance (See Text for a Full Description) for the Decision Tree Model*

Prediction factor	Multiple linear regression (coefficient)	Decision tree (predictor importance ×1,000)
Phosphate	1.3	0.4
Nitrate	−0.4	3.4
Silicate	1.4	0.6
Oxygen	0.2	0.02
Temperature	−0.2	0.08
Salinity	−0.2	0.2
Depth	−0.2	0.008
Sine latitude	−0.001	0.02
Cosine latitude	0.2	0.01

*Note.* Values are reported as the outcome of models trained on the full data set containing all GEOTRACES Ni observations.

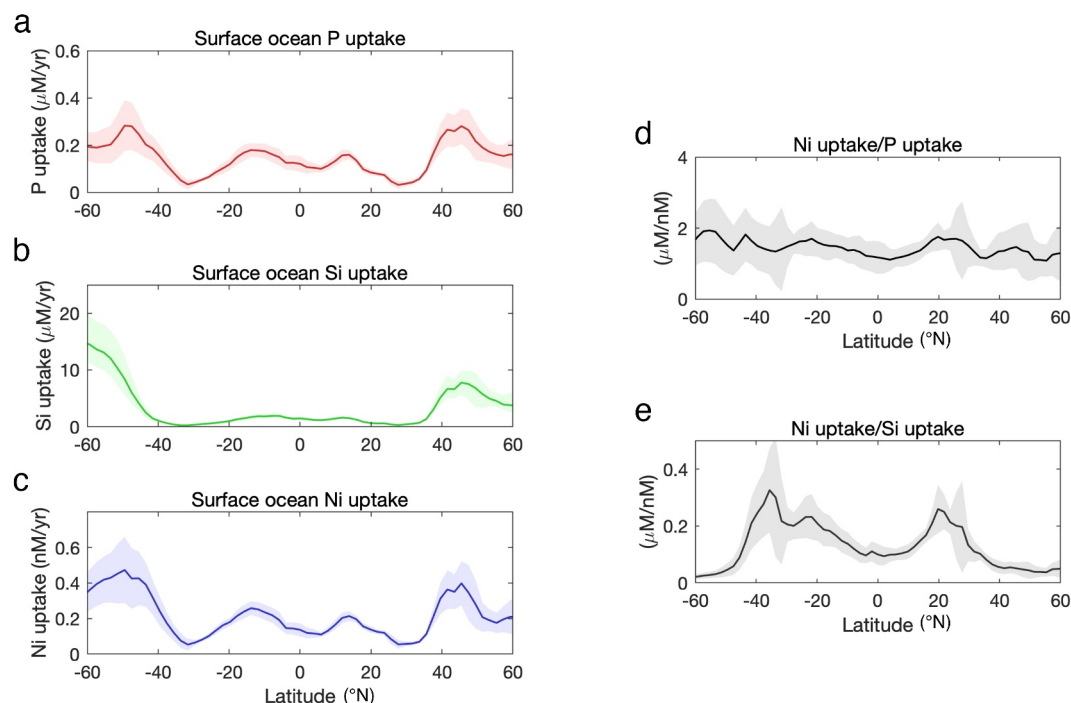


**Figure 7.** Global meridional mean nutrient transport convergences in the surface ocean, interpreted here as reflecting the biological uptake of phosphate (a), silicate (b), and nickel (c). Also shown are the relative rates of Ni/P uptake (d) and Ni/Si uptake (e). Shaded regions represent the  $1\sigma$  standard deviation across the 200 different nutrient restoring models used in this study.

conclusions from previous work suggesting that most biologically cycled Ni is not present in diatom frustules (John et al., 2022). If frustule-associated Ni were an important driver of upper ocean Ni distributions, we would expect that surface uptake patterns of Ni would be more similar to those of Si, while in fact we find that surface ocean Ni uptake patterns are more similar to P.

Phosphate and Ni uptake patterns in the surface ocean also support our previous work suggesting that there is not a  $\sim 2$  nM pool of non-bioavailable Ni. If such a pool were present, we would expect Ni/P uptake ratios to decrease dramatically as Ni concentrations approach 2 nM, because phytoplankton metal/P uptake quotas are typically nearly linearly dependent on the concentration of bioavailable metal. This has been demonstrated for Ni in laboratory cultures of both diatoms (Egleston & Morel, 2008) and cyanobacteria (Dupont et al., 2008; Ho, 2013). However, the uptake of Ni and P in the surface ocean instead shows a slight increase in Ni/P uptake ratios in parts of the surface ocean where Ni concentrations are near 2 nM, though the differences in uptake rates are not significantly different for any Ni concentration (Figure 8).

The surface ocean Ni/P uptake rates inferred from the model, which are generally  $1\text{--}2$  nmol/ $\mu\text{mol}$  (Figures 7 and 8), can be compared to in situ measurements of particle stoichiometry. Most SXRF analyses of Ni/P in individual phytoplankton cells are notably lower. For example, measurements of autotrophic flagellated cells and picoplankton in the low-latitude oceans have Ni/P around 0.2 to 0.6, as do diatoms in the temperate Pacific Ocean (Twining & Baines, 2013; Twining et al., 2011). Only diatoms in the Equatorial and Southern Oceans have higher Ni/P of around 0.5 to 1.5 (Twining & Baines, 2013; Twining et al., 2004). Measurements of bulk particulate stoichiometry range widely, from 0.21 for a diatom bloom in Monterey Bay (Martin & Knauer, 1973), to as high as 8.1 for North Atlantic samples rich in *Trichodesmium* (Nuester et al., 2012), with many intermediate values between 0.68 and 1.4 reported for various ocean locations (Collier & Edmond, 1984; Kuss & Kremling, 1999; Tovar-Sanchez et al., 2006). Thus, our model-derived estimates of surface ocean Ni/P uptake are within the range measured for in situ marine phytoplankton and plankton assemblages, though we note that the higher Ni/P ratios are generally associated with diatoms and *Trichodesmium*. It therefore seems likely that such species with higher Ni/P have an outsized impact on the surface uptake of Ni.

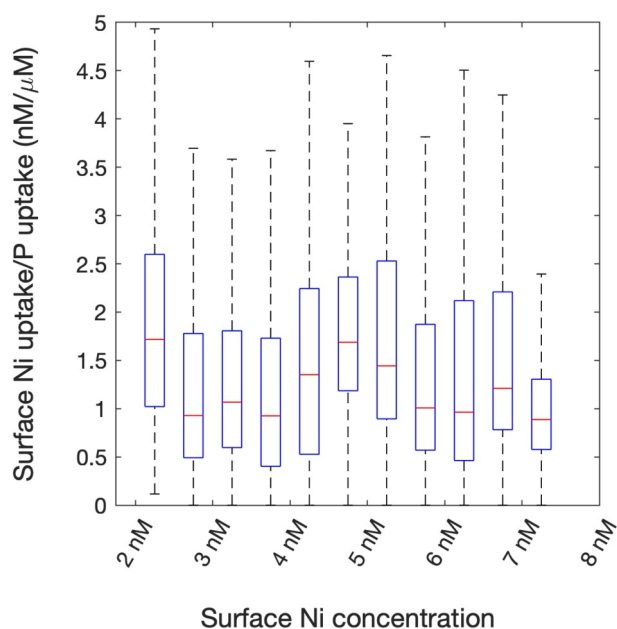


**Figure 8.** The ratio of Ni uptake to P uptake in the surface oceans is binned based on Ni concentration, in order to show that the relative Ni uptake rates do not decrease as Ni approaches 2 nM. Shown are the median value (red lines), 25th and 75th percentile (blue boxes), and total extent of the data (black dashed lines).

### 3.3. Regeneration of Ni in the Deep Oceans

Flux divergences of Ni, phosphate, and silicate are positive in the deep ocean, indicating local biogeochemical sources that we interpret as nutrient regeneration from sinking particles (Figures 6 and 9). For silicate, this regeneration is interpreted as the dissolution of diatom frustules, while for phosphate it is interpreted as the remineralization of sinking organic matter. As expected from the presence of Si within the refractory matrix of diatom frustules, silicate is regenerated much more deeply in the water column than phosphate. For example, 77% of P regeneration occurs above 1,000 m depth and 93% occurs above 3,000 m depth, while for Si these proportions are just 36% and 68%, respectively. The regeneration depth of Ni is intermediate between that of Si and that of P, with 58% and 86% of regeneration occurring above 1,000 and 3,000 m, respectively.

This correlation of Ni with both P and Si was noted in the first studies that accurately measured Ni in seawater (Bruland, 1980; Sclater et al., 1976). At the time it was suggested that this could reflect two different remineralization length scales for Ni though a number of different reasons have since been proposed to explain this observation. For example, it has been suggested that diatoms contain significant Ni within their frustules, which would mean that soft-tissue phytoplankton Ni regenerates with P in the upper water column, while the Ni contained within the frustules regenerates deeper in the water column along with Si (Twining et al., 2012). However, as discussed above, previous work shows that neither cultured diatoms nor natural ocean diatoms contain a significant amount of Ni within their silicate frustules (John et al., 2022). Additionally, the results of our diagnostic modeling presented here show that Ni uptake is more closely coupled to P than to Si. Because

biological Ni is thought to be located mostly at the active site of metalloenzymes, it is expected to be released from cells during the regeneration of macronutrients N and P. Thus, if biological uptake of Ni into soft tissue and remineralization of that Ni were the only processes by which Ni is regenerated, we would expect its regeneration profile to look very similar to that of P. Possible explanations for the deeper regeneration of Ni include a high stoichiometric proportion of Ni in a class of organisms which remineralizes more deeply in the water column such as rapidly sinking diatoms, the presence of a presently unknown refractory phase of biological Ni, or the reversible scavenging onto sinking particles, which acts to slowly remove metals from the upper ocean and release them again in the deeper ocean, such that net regeneration of Ni occurs deeper in the ocean than for P (John et al., 2022).

Although previous studies of Ni cycling have mostly invoked vertical transport with sinking particles taking Ni deeper into the ocean than P as the reason for the similarities between Ni and Si, it should be noted that differences in surface uptake patterns can also impact vertical distributions in the oceans as waters mix into the deep ocean, primarily along isopycnals (Sarmiento et al., 2004). We have therefore calculated the preformed and regenerated P, Si, and Ni concentrations in order to better delineate differences in vertical particle transport from circulation (Figure 10). While transport convergences provide the net in situ rates at which elements are regenerated, the regenerated fraction of Ni can be calculated from the Ni climatology and circulation transport matrix alone. The preformed Ni is determined as the portion of Ni which can be attributed to circulation from surface-ocean grid cells, and the rest of the Ni is attributed to regeneration. Such a comparison of preformed and regenerated nutrients illustrates the integrated impact of regeneration on elemental concentration over the entire timescale of deep-ocean transport and mixing. Again, we see a pattern whereby Ni regeneration appears to lie between P and Si. By subtracting preformed from total concentrations, we can isolate the portion attributable to regeneration. Regenerated P has a distinct maximum in the upper ocean around 1,000 m. In contrast, regenerated Si increases toward the deep ocean, with highest values observed in the abyssal ocean. The depth distribution of regenerated Ni is intermediate between these two extremes, as inferred from the earliest measurements of Ni in seawater (Bruland, 1980; Sclater et al., 1976).

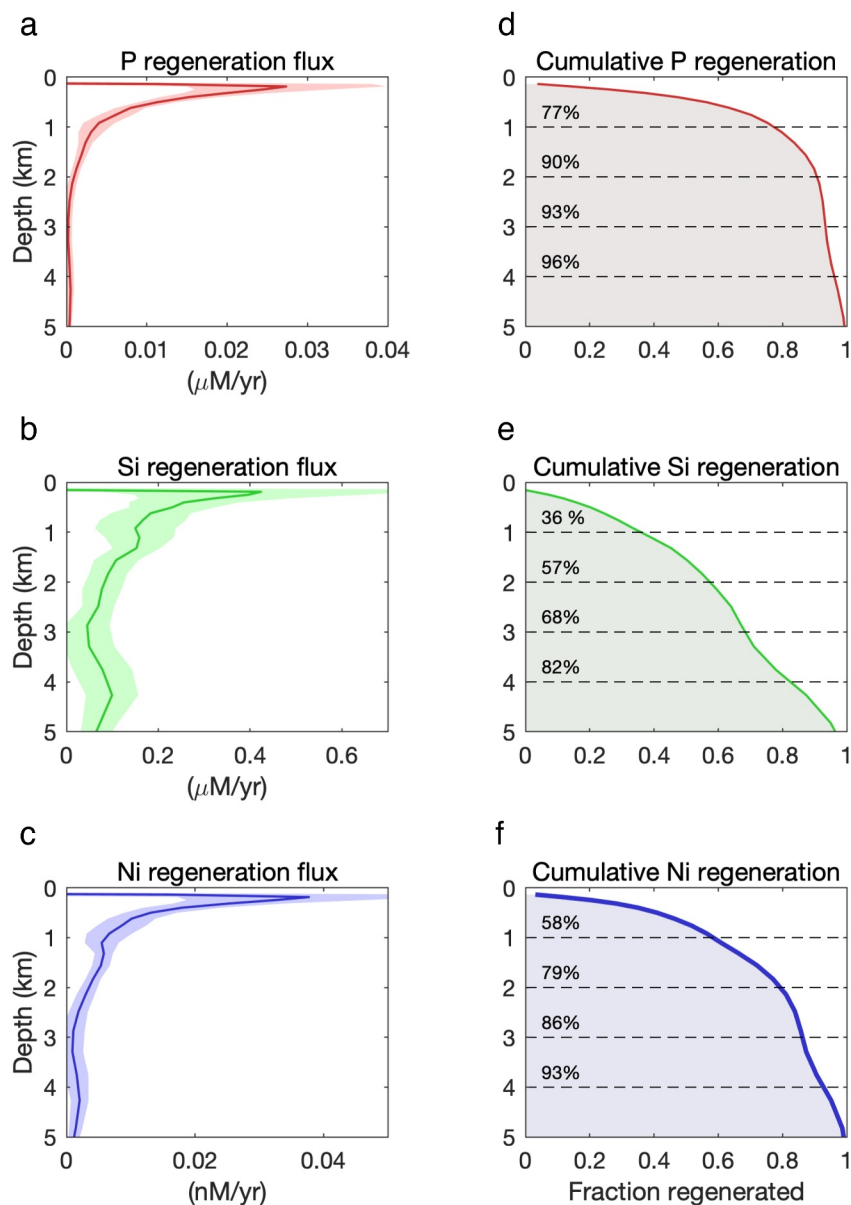


**Figure 9.** Global average depth profiles of the nutrient transport divergence, interpreted here as reflecting the net regeneration of phosphate, silicate, and nickel, where the shaded regions represent the  $1\sigma$  standard deviation across the 200 different nutrient restoring models used for this study (a–c). Each profile is also summed and normalized to the total regeneration flux in order to show the cumulative regeneration with depth (d–f).

#### 4. Conclusions

An earlier mechanistic (prognostic) model of marine Ni cycling highlighted several important processes that control the distribution of nickel in the global oceans. These include slower uptake of Ni compared to macronutrients from upwelling waters, slow Ni regeneration or reversible scavenging of Ni onto sinking particles, and the absence of a non-bioavailable form of Ni in the surface oceans (John et al., 2022). The work presented here complements our previous findings using a very different approach. Here we inferred the processes that control the spatial distribution of Ni in the oceans by diagnosing the transport divergences of Ni, without first making any assumptions about the biogeochemical processes that might underlie Ni distributions.

The diagnostic modeling approach taken here largely supports the results of the earlier prognostic approach. We find strongly co-located patterns of Ni uptake and P uptake in the surface ocean, with both elements taken up

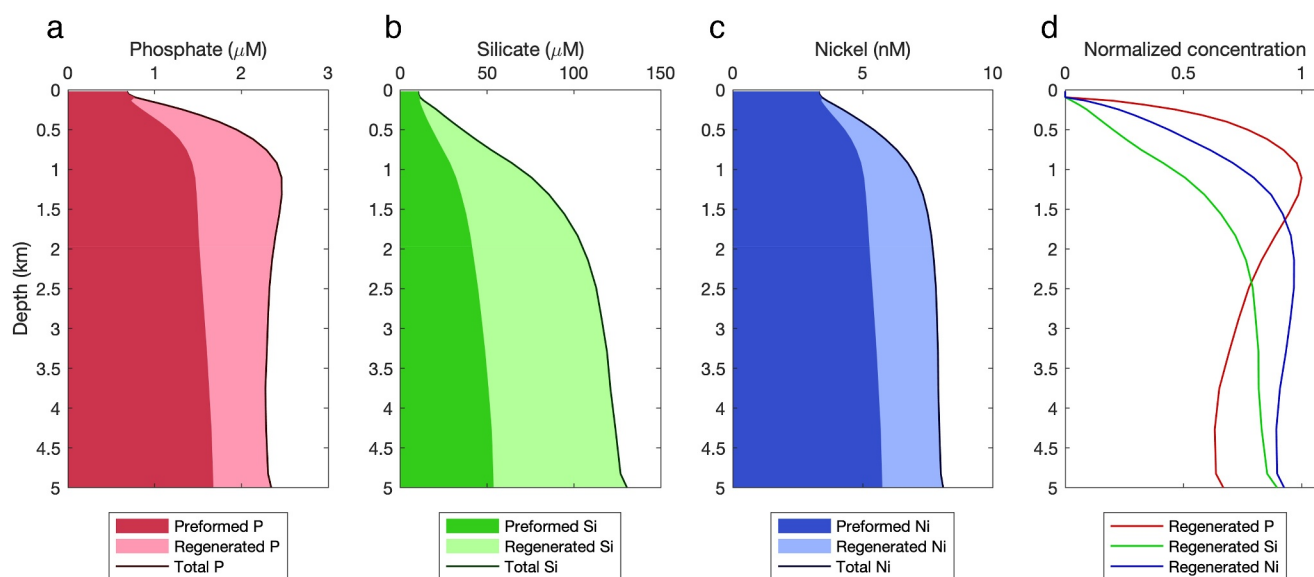


**Figure 10.** Globally averaged preformed and regenerated concentrations of phosphate, silicate, and nickel are shown as the darker and lighter shaded areas, respectively, while the total concentrations plotted as dark lines are simply the sum of these two (a–c). The global average concentrations of regenerated phosphate, silicate, and nickel are also plotted together in order to better compare their depth distributions normalized to the maximum concentration (d).

much more substantially at lower latitudes compared to Si, which is depleted at higher latitudes, consistent with the assumption of our previous mechanistic model that Ni is not present in diatom frustules. We also find that Ni regeneration occurs deeper in the water column than for P, though not as deep as for Si, which is consistent with the assumption of our previous mechanistic model that Ni is brought deeper into the ocean either due to slower Ni remineralization compared to P or via reversible scavenging.

An important methodological finding is multiple linear regression (MLR) is a better tool compared to artificial neural networks (ANNs) and decision trees for predicting Ni concentrations in regions far from the training region. While ANNs and decision trees produced spurious data and were prone to overfitting, the MLR method performed better overall. Although complicated machine learning techniques have been successfully used to predict trace-element climatologies in the past (Huang et al., 2022; Mete et al., 2023; Roshan & DeVries, 2021; Roshan et al., 2018, 2020). Our work highlights potential concerns with this method and suggests that in some cases simpler approaches, such as MLR, may be more appropriate.

Finally, we hope that this manuscript will serve as a useful guide for other researchers with an interest in the diagnostic modeling techniques used here. This follows in the footsteps of other recent projects such as the AWESOME OCIM (S. G. John et al., 2020), which aims to put OCIM modeling tools in the hands of non-expert modelers, and AIBECS (Pasquier, 2019; Pasquier et al., 2022), which follows a similar approach but includes more sophisticated modeling tools, non-linear solvers, and is written in the open-source Julia language. As much as possible, this manuscript has been written in a language approachable to an audience without a strong background in mathematics and coding, as there are other manuscripts which present the same techniques in a more mathematically focused fashion (Roshan & DeVries, 2017, 2021; Roshan et al., 2018, 2020). With the advent of global-scale sampling projects such as GEOTRACES (Anderson, 2019) and BioGeoSCAPES, we anticipate a greater need for tools which facilitate the use of models by scientists with a background in fieldwork and sample analysis, and hope that this manuscript will aid in that effort.

### Data Availability Statement

All code used in this project is available on Zenodo at <https://doi.org/10.5281/zenodo.10689935> (John, 2024).

## Acknowledgments

This work was funded by the National Science Foundation (2049639 to SGJ), the Simons Foundation (426570SP and LI-SIAME-00001532 to SGJ), and Australian Research Council (DP210101650 to MH).

## References

- Alfano, M., & Cavazza, C. (2020). Structure, function, and biosynthesis of nickel-dependent enzymes. *Protein Science*, 29(5), 1071–1089. <https://doi.org/10.1002/pro.3836>
- Anderson, R. F. (2019). GEOTRACES: Accelerating research on the marine biogeochemical cycles of trace elements and their isotopes. *Annual Review of Marine Science*, 12(1), 49–85. <https://doi.org/10.1146/annurev-marine-010318-095123>
- Archer, C., Vance, D., Milne, A., & Lohan, M. C. (2020). The oceanic biogeochemistry of nickel and its isotopes: New data from the South Atlantic and the Southern Ocean biogeochemical divide. *Earth and Planetary Science Letters*, 535, 116118. <https://doi.org/10.1016/j.epsl.2020.116118>
- Biscéré, T., Ferrier-Pagès, C., Grover, R., Gilbert, A., Rottier, C., Wright, A., et al. (2018). Enhancement of coral calcification via the interplay of nickel and urease. *Aquatic Toxicology*, 200, 247–256. <https://doi.org/10.1016/j.aquatox.2018.05.013>
- Boiteau, R. M., Till, C. P., Ruacho, A., Bundy, R. M., Hawco, N. J., McKenna, A. M., et al. (2016). Structural characterization of natural nickel and copper binding ligands along the US GEOTRACES Eastern Pacific zonal transect. *Frontiers in Marine Science*, 3. <https://doi.org/10.3389/fmars.2016.00243>
- Bruland, K. W. (1980). Oceanographic distributions of cadmium, zinc, nickel, and copper in the North Pacific. *Earth and Planetary Science Letters*, 47(2), 176–198. [https://doi.org/10.1016/0012-821x\(80\)90035-7](https://doi.org/10.1016/0012-821x(80)90035-7)
- Collier, R., & Edmond, J. (1984). The trace element geochemistry of marine biogenic particulate matter. *Progress in Oceanography*, 13(2), 113–199. [https://doi.org/10.1016/0079-6611\(84\)90008-9](https://doi.org/10.1016/0079-6611(84)90008-9)
- DeVries, T. (2014). The oceanic anthropogenic CO<sub>2</sub> sink: Storage, air-sea fluxes, and transports over the industrial era. *Global Biogeochemical Cycles*, 28(7), 631–647. <https://doi.org/10.1002/2013gb004739>
- DeVries, T., & Holzer, M. (2019a). Radiocarbon and helium isotope constraints on deep ocean ventilation and Mantle-3He sources. *Journal of Geophysical Research: Oceans*, 124(5), 3036–3057. <https://doi.org/10.1029/2018jc014716>
- DeVries, T., & Holzer, M. (2019b). Radiocarbon and helium isotope constraints on deep ocean ventilation and Mantle-3He sources. *Journal of Geophysical Research: Oceans*, 124(5), 3036–3057. <https://doi.org/10.1029/2018jc014716>
- DeVries, T., & Primeau, F. (2011). Dynamically and observationally constrained estimates of water-mass distributions and ages in the global ocean. *Journal of Physical Oceanography*, 41(12), 2381–2401. <https://doi.org/10.1175/jpo-d-10-05011.1>
- Dupont, C. L., Barbeau, K., & Palenik, B. (2008). Ni uptake and limitation in marine synechococcus strains. *Applied and Environmental Microbiology*, 74(1), 23–31. <https://doi.org/10.1128/aem.01007-07>
- Egleston, E. S., & Morel, F. M. M. (2008). Nickel limitation and zinc toxicity in a urea-grown diatom. *Limnology & Oceanography*, 53(6), 2462–2471. <https://doi.org/10.4319/lo.2008.53.6.2462>
- GEOTRACES Intermediate Data Product Group. (2021). The GEOTRACES intermediate data product 2021 (IDP2021). *NERC EDS British Oceanographic Data Centre NOC*. <https://doi.org/10.5285/cf2d9ba9-d51d-3b7c-e053-8486abc0f5fd>
- Grist, J. P., Josey, S. A., Marsh, R., Good, S. A., Coward, A. C., de Cuevas, B. A., et al. (2010). The roles of surface heat flux and ocean heat transport convergence in determining Atlantic Ocean temperature variability. *Ocean Dynamics*, 60(4), 771–790. <https://doi.org/10.1007/s10236-010-0292-4>
- Ho, T.-Y. (2013). Nickel limitation of nitrogen fixation in Trichodesmium. *Limnology & Oceanography*, 58(1), 112–120. <https://doi.org/10.4319/lo.2013.58.1.0112>
- Huang, Y., Tagliabue, A., & Cassar, N. (2022). Data-driven modeling of dissolved iron in the global ocean. *Frontiers in Marine Science*, 9. <https://doi.org/10.3389/fmars.2022.837183>
- John, S. G. (2024). MTEL-USC/nickel-diagnostic-model: v2 (version v2) [Software]. *Zenodo*. <https://doi.org/10.5281/zenodo.10689935>
- John, S. G., & Sunda, W. (2018). Trace metal nutrients. In J. K. Cochran, H. J. Bokuniewicz, & P. L. Yager (Eds.), *Encyclopedia of ocean sciences* (3rd ed., pp. 208–217). Elsevier.
- John, S. G., Kelly, R. L., Bian, X., Fu, F., Smith, M. I., Lanning, N. T., et al. (2022). The biogeochemical balance of oceanic nickel cycling. *Nature Geoscience*, 15(11), 906–912. <https://doi.org/10.1038/s41561-022-01045-7>
- John, S. G., Liang, H., Weber, T., DeVries, T., Primeau, F., Moore, K., et al. (2020a). AWESOME OCIM: A simple, flexible, and powerful tool for modeling elemental cycling in the oceans. *Chemical Geology*, 533, 119403. <https://doi.org/10.1016/j.chemgeo.2019.119403>
- John, S. G., Liang, H., Weber, T., DeVries, T., Primeau, F., Moore, K., et al. (2020b). AWESOME OCIM: A simple, flexible, and powerful tool for modeling elemental cycling in the oceans. *Chemical Geology*, 533, 119403. <https://doi.org/10.1016/j.chemgeo.2019.119403>
- Konhäuser, K. O., Pecoits, E., Lalonde, S. V., Papineau, D., Nisbet, E. G., Barley, M. E., et al. (2009). Oceanic nickel depletion and a methanogen famine before the Great Oxidation Event. *Nature*, 458(7239), 750–753. <https://doi.org/10.1038/nature07858>
- Kuss, J., & Kremling, K. (1999). Spatial variability of particle associated trace elements in near-surface waters of the North Atlantic (30°N/60°W to 60°N/2°W), derived by large volume sampling. *Marine Chemistry*, 68(1–2), 71–86. [https://doi.org/10.1016/s0304-4203\(99\)00066-3](https://doi.org/10.1016/s0304-4203(99)00066-3)
- Lemaître, N., Du, J., de Souza, G. F., Archer, C., & Vance, D. (2022). The essential bioactive role of nickel in the oceans: Evidence from nickel isotopes. *Earth and Planetary Science Letters*, 584, 117513. <https://doi.org/10.1016/j.epsl.2022.117513>
- Little, S. H., Archer, C., McManus, J., Najorka, J., Wegorzewski, A. V., & Vance, D. (2020). Towards balancing the oceanic Ni budget. *Earth and Planetary Science Letters*, 547, 116461. <https://doi.org/10.1016/j.epsl.2020.116461>
- Mackey, D. J., O'Sullivan, J. E., Watson, R. J., & Dal Pont, G. (2002). Trace metals in the Western Pacific: Temporal and spatial variability in the concentrations of Cd, Cu, Mn and Ni. *Deep-Sea Research Part I Oceanographic Research Papers*, 49(12), 2241–2259. [https://doi.org/10.1016/s0967-0637\(02\)00124-3](https://doi.org/10.1016/s0967-0637(02)00124-3)
- Martin, J. H., & Knauer, G. A. (1973). The elemental composition of plankton. *Geochimica et Cosmochimica Acta*, 37(7), 1639–1653. [https://doi.org/10.1016/0016-7037\(73\)90154-3](https://doi.org/10.1016/0016-7037(73)90154-3)
- Mete, Ö. Z., Subhas, A. V., Kim, H. H., Dunlea, A. G., Whitmore, L. M., Shiller, A. M., et al. (2023). Barium in seawater: Dissolved distribution, relationship to silicon, and barite saturation state determined using machine learning. *Earth System Science Data*, 15(9), 4023–4045. <https://doi.org/10.5194/essd-15-4023-2023>
- Middag, R., de Baar, H. J. W., Bruland, K. W., & van Heuven, S. M. A. C. (2020). The distribution of nickel in the West-Atlantic Ocean, its relationship with phosphate and a comparison to cadmium and zinc. *Frontiers in Marine Science*, 7, 105. <https://doi.org/10.3389/fmars.2020.00105>
- Minami, T., Konagaya, W., Zheng, L., Takano, S., Sasaki, M., Murata, R., et al. (2015). An off-line automated preconcentration system with ethylenediaminetriacetate chelating resin for the determination of trace metals in seawater by high-resolution inductively coupled plasma mass spectrometry. *Analytica Chimica Acta*, 854, 183–190. <https://doi.org/10.1016/j.aca.2014.11.016>
- Nuester, J., Vogt, S., Newville, M., Kustka, A., & Twining, B. (2012). The unique biogeochemical signature of the marine diazotroph Trichodesmium. *Frontiers in Microbiology*, 3, 150. <https://doi.org/10.3389/fmicb.2012.00150>

- Pasquier, B. (2019). AIBECs.jl: The ideal tool for simple global marine biogeochemistry models.
- Pasquier, B., Primeau, F. W., & John, S. G. (2022). AIBECs.jl: A tool for exploring global marine biogeochemical cycles. *Journal of Open Source Software*, 7(69), 3814. <https://doi.org/10.21105/joss.03814>
- Price, N. M., & Morel, F. M. M. (1991). Colimitation of phytoplankton growth by nickel and nitrogen. *Limnology & Oceanography*, 36(6), 1071–1077. <https://doi.org/10.4319/lo.1991.36.6.1071>
- Qiu, B., & Price, N. M. (2009). Different physiological responses of four marine *Synechococcus* strains (cyanophyceae) to nickel starvation under iron-replete and iron-deplete conditions. *Journal of Phycology*, 45(5), 1062–1071. <https://doi.org/10.1111/j.1529-8817.2009.00732.x>
- Roshan, S., & DeVries, T. (2017). Efficient dissolved organic carbon production and export in the oligotrophic ocean. *Nature Communications*, 8(1), 2036. <https://doi.org/10.1038/s41467-017-02227-3>
- Roshan, S., & DeVries, T. (2021). Global contrasts between oceanic cycling of cadmium and phosphate. *Global Biogeochemical Cycles*, 35(6), e2021GB006952. <https://doi.org/10.1029/2021gb006952>
- Roshan, S., DeVries, T., & Wu, J. (2020). Constraining the global oceanic Cu cycle with a data-assimilated diagnostic model. *Global Biogeochemical Cycles*, 34(11), e2020GB006741. <https://doi.org/10.1029/2020gb006741>
- Roshan, S., DeVries, T., Wu, J., & Chen, G. (2018). The internal cycling of zinc in the ocean. *Global Biogeochemical Cycles*, 32(12), 1833–1849. <https://doi.org/10.1029/2018gb006045>
- Roshan, S., & Wu, J. (2015). The distribution of dissolved copper in the tropical-subtropical north Atlantic across the GEOTRACES GA03 transect. *Marine Chemistry*, 176, 189–198. <https://doi.org/10.1016/j.marchem.2015.09.006>
- Sarmiento, J. L., Gruber, N., Brzezinski, M. A., & Dunne, J. P. (2004). High-latitude controls of thermocline nutrients and low latitude biological productivity. *Nature*, 427(6969), 56–60. <https://doi.org/10.1038/nature02127>
- Schlitzer, R., Anderson, R. F., Dodas, E. M., Lohan, M., Geibert, W., Tagliabue, A., et al. (2018). The GEOTRACES intermediate data product 2017. *Chemical Geology*, 493, 210–223. <https://doi.org/10.1016/j.chemgeo.2018.05.040>
- Sclater, F. R., Boyle, E., & Edmond, J. M. (1976). On the marine geochemistry of nickel. *Earth and Planetary Science Letters*, 31(1), 119–128. [https://doi.org/10.1016/0012-821x\(76\)90103-5](https://doi.org/10.1016/0012-821x(76)90103-5)
- Sutton, R., & Mathieu, P.-P. (2002). Response of the atmosphere–ocean mixed-layer system to anomalous ocean heat-flux convergence. *Quarterly Journal of the Royal Meteorological Society*, 128(582), 1259–1275. <https://doi.org/10.1256/003590002320373283>
- Tovar-Sanchez, A., Sañudo-Wilhelmy, S. A., Kustka, A. B., Agustí, S., Dachs, J., Hutchins, D. A., et al. (2006). Effects of dust deposition and river discharges on trace metal composition of *Trichodesmium* spp. in the tropical and subtropical North Atlantic Ocean. *Limnology & Oceanography*, 51(4), 1755–1761. <https://doi.org/10.4319/lo.2006.51.4.1755>
- Tuo, S., Rodriguez, I. B., & Ho, T.-Y. (2020). H<sub>2</sub> accumulation and N<sub>2</sub> fixation variation by Ni limitation in *Cyanothece*. *Limnology & Oceanography*, 65(2), 377–386. <https://doi.org/10.1002/lno.11305>
- Twining, B. S., & Baines, S. B. (2013). The trace metal composition of marine phytoplankton. *Annual Review of Marine Science*, 5(1), 191–215. <https://doi.org/10.1146/annurev-marine-121211-172322>
- Twining, B. S., Baines, S. B., Bozard, J. B., Vogt, S., Walker, E. A., & Nelson, D. M. (2011). Metal quotas of plankton in the equatorial Pacific Ocean. *Deep Sea Research Part II: Topical Studies in Oceanography*, 58(3–4), 325–341. <https://doi.org/10.1016/j.dsr2.2010.08.018>
- Twining, B. S., Baines, S. B., & Fisher, N. S. (2004). Element stoichiometries of individual plankton cells collected during the Southern Ocean Iron Experiment (SOFEX). *Limnology & Oceanography*, 49(6), 2115–2128. <https://doi.org/10.4319/lo.2004.49.6.2115>
- Twining, B. S., Baines, S. B., Vogt, S., & Nelson, D. M. (2012). Role of diatoms in nickel biogeochemistry in the ocean. *Global Biogeochemical Cycles*, 26(4). <https://doi.org/10.1029/2011gb004233>
- Wang, S.-J., Rudnick, R. L., Gaschnig, R. M., Wang, H., & Wasylenki, L. E. (2019). Methanogenesis sustained by sulfide weathering during the great oxidation event. *Nature Geoscience*, 12(4), 296–300. <https://doi.org/10.1038/s41561-019-0320-z>
- Weber, T. S., Cram, J. A., Leung, S. W., DeVries, T., & Deutsch, C. (2016). Deep ocean nutrients imply large latitudinal variation in particle transfer efficiency. *Proceedings of the National Academy of Sciences of the United States of America*, 113(31), 8606–8611. <https://doi.org/10.1073/pnas.1604414113>
- Weber, T. S., & Deutsch, C. (2010). Ocean nutrient ratios governed by plankton biogeography. *Nature*, 467(7315), 550–554. <https://doi.org/10.1038/nature09403>
- Wen, L.-S., Jiann, K.-T., & Santschi, P. H. (2006). Physicochemical speciation of bioactive trace metals (Cd, Cu, Fe, Ni) in the oligotrophic South China Sea. *Marine Chemistry*, 101(1–2), 104–129. <https://doi.org/10.1016/j.marchem.2006.01.005>
- Zanna, L., Khaliwala, S., Gregory, J. M., Ison, J., & Heimbach, P. (2019). Global reconstruction of historical ocean heat storage and transport. *Proceedings of the National Academy of Sciences of the United States of America*, 116(4), 1126–1131. <https://doi.org/10.1073/pnas.1808838115>
- Zhao, Z., Shen, B., Zhu, J.-M., Lang, X., Wu, G., Tan, D., et al. (2021). Active methanogenesis during the melting of Marinoan snowball Earth. *Nature Communications*, 12(1), 955. <https://doi.org/10.1038/s41467-021-21114-6>
- Zheng, L., Minami, T., Takano, S., Ho, T.-Y., & Sohrin, Y. (2021). Sectional distribution patterns of Cd, Ni, Zn, and Cu in the North Pacific Ocean: Relationships to nutrients and importance of scavenging. *Global Biogeochemical Cycles*, 35(7), e2020GB006558. <https://doi.org/10.1029/2020gb006558>